Korean J. Chem. Eng., 39(10), 2792-2799 (2022)
DOI: 10.1007/s11814-022-1143-y

pISSN: 0256-1115
eISSN: 1975-7220

Renewable magnetic alginate-graphene oxide hybrid for efficient cationic dye removal

Wenju Liu, Hongjuan Bai, Weiqiang Gao, Zihan Chen, Zhuangzhuang Liu, Zilong Chen, and Junhang Chen†

School of Chemistry and Chemical Engineering, Henan University of Technology, Zhengzhou 450001, P. R. China
(*Received 9 February 2022 • Revised 4 April 2022 • Accepted 10 April 2022*)

Abstract−A batch system was applied to investigate the behavior of adsorption of methylene blue (MB) and crystal violet (CV) from aqueous solution using a renewable magnetic alginate composite containing graphene oxide (M-GO/Alg) in single and binary systems. The surface morphology and chemical structure of the adsorbent were characterized by scanning electron microscopy (SEM), X-ray diffraction (XRD), thermogravimetric analysis (TGA), and vibrating sample magnetometer (VSM) analysis. The experimental data were fitted by the isotherm models and adsorption kinetics. And the maximum adsorption quantity of MB and CV reached 459.85 and 69.46 mg/g at 298 K for M-GO/Alg, respectively, as deduced from Langmuir model. After five successive adsorptive removal cycles for both dyes, no significant performance loss was observed for M-GO/Alg. Moreover, M-GO/Alg was easily separated under an external magnetic field. In binary system, MB and CV exhibited competitive adsorption. The obtained results suggested that M-GO/Alg can be used as an eco-friendly and recyclable adsorbent to remove cationic dyes from aqueous solutions.

Keywords: Graphene Oxide, Alginate, Adsorption, Cationic Dye, Magnetic Separation

INTRODUCTION

Water pollution from synthetic organic dyes (including cationic dyes) and the treatment of dye-contaminated water has become worldwide environmental issues [1]. Organic dyes pose potential threats to the environment because of their toxicity, persistence, and bioaccumulation [2-6]. For example, methylene blue (MB), a colorant and disinfector, is found in various industrial effluents (dyestuffs, rubbers, pesticides, pharmaceuticals, and varnishes) [7-9] that poses a threat to ecological environments and human health [9]. Crystal violet dye (CV) is a water-soluble cationic triphenyl methane dye widely used in various medical fields as an active ingredient in Gram's stain, a bacteriostatic agent, and an external skin disinfectant [10]. And the dye is well-known to be unsafe, carcinogenic, mutagenic [11]. It can be absorbed through the skin, inhalation and ingestion, causing horrible irritation and painful sensitization [12]. Thus, there is a need to eliminate such cationic dyes from industrial effluents before they are discharged into water bodies [13,14]. Different techniques have been developed to treat wastewater containing dyes, including membrane filtration, ion-exchange, adsorption, activated sludge, and bacterial action methods [15-19]. Among these, adsorption is always considered because of its easy operation, low cost, and high sorption efficiency [20-24].

Graphene oxide (GO), consisting of one-carbon-atom-thick planar nanosheets, has been widely used as an adsorbent to eliminate contaminants from aqueous solutions [25]. Many function groups (for example, hydroxyl, epoxy, and carboxyl) exist on the surfaces and edges of GO [26]. These functional groups can interact with adsorbates through electrostatic interaction and hydrogen bonding [25,27]. However, when used as an adsorbent, it is difficult to separate GO from water and may require inconvenient high-speed centrifugation [28]. Magnetic nanoparticles have been proposed as a means to solve this problem and enhance the recoverability using a magnet [29,30]. Fe_3O_4 nanoparticles are extensively used as magnetic materials due to their high surface area, biocompatibility, easy magnetic separation and low ecotoxicity [31]. However, they also have some disadvantages, for example, Fe_3O_4 nanoparticles are prone to aggregating in solutions, and easy oxidation, corrosion and release metal ions [32-34]. To improve the stability of magnetic materials, they can be dispersed onto other materials to form composites [35,36].

Sodium alginate is a natural polysaccharide that can easily chelate with divalent cations to form 3D macro-composites through tightly-bonded junctions [37]. Sodium alginate has been used to develop adsorbents for wastewater treatment due to its biodegradability, water solubility, multiple functional groups, and non-ecotoxicity [38,39]. Alginate has also been used to immobilize hectorite clay [38], multiwalled carbon nanotubes [32,40], SiO_2 nanoparticles [30], and activated carbon [41] to form adsorbents employed for the removal of dyes or heavy metals from aqueous solutions. Composite materials prepared from GO and alginate have been used as adsorbents to remove contaminations (dyes or/and heavy metals) from wastewater [38-41]. However, to our best knowledge, few studies have reported the simultaneous removal of cationic dyes using alginate composite beads containing magnetic iron oxide nanoparticles and graphene oxide (M-GO/Alg) from aqueous solutions.

This study aimed to prepare a benign, efficient, and easily and repeatedly recycled magnetic adsorbent to remove cationic dyes of MB and CV from aqueous solutions. To that end, magnetic alginate beads consisting of Fe_3O_4 nanoparticles and GO were prepared, characterized, and used to adsorb MB and CV in single and binary dye systems. The removal of MB and CV dyes pro-

†To whom correspondence should be addressed.
E-mail: chenjunhang@haut.edu.cn

cesses was deduced by the parameters obtained from the kinetics and adsorption isotherm models. The recovery of MB and CV from the beads after adsorption was also performed.

EXPERIMENTAL PROCEDURES

1. Reagents and Solutions

Methylene blue (FW=373.9), Crystal violet (FW=570.1) and Fe_3O_4 nanoparticles were obtained from Aladdin®. Other chemicals were analytical-grade and purchased from Macklin®. All solutions were prepared with ultrapure water (EASYPure II water system, Iowa, USA).

2. Preparation of GO and Magnetic-GO/Alg Beads (M-GO/Alg)

A modified Hummers' method [42] was employed to prepare GO: Briefly, 1 g graphite was mixed with 23 mL H_2SO_4, 2 mL H_3PO_4, and 6 g $KMnO_4$ in a 500 mL flask on an ice bath with continuous stirring. The mixture above was stirred for 2 h at 35 °C. A brownish paste was obtained as the reaction progressed. Then, pure water (50 mL) was added into the mixture. The reaction mixture was rapidly heated to 98 °C for 15 min. To terminate the reaction, H_2O_2 was slowly added into the mixture with a bright-yellow color. After centrifugation, the precipitate was washed thoroughly and dried in an oven at 80 °C, finally, GO was obtained.

A 0.25 g sample of GO and 0.7 g Fe_3O_4 nanoparticles were dispersed into 50 mL of distilled water, and a homogeneous dispersion was obtained via ultrasonication for 30 min. Then, 1 g sodium alginate was dissolved in the 50 mL homogeneous dispersion with continuous stirring for 2 h. Dropping the magnetic dispersion into a 1 mol/L calcium chloride solution, which used as the curing agent with gentle agitation for 2 h, formed magnetic GO/Fe_3O_4/Alg composite beads (designed as M-GO/Alg). The beads were kept in the calcium chloride solution and after 12 h, the beads were washed thoroughly with distilled water. Finally, the beads were dried for 6 h.

3. Characterization

The morphology of GO, GO/Alg, and M-GO/Alg was studied by SEM (ZEISS MERLIN Compact, Germany). XRD patterns of GO/Alg and M-GO/Alg were observed by an X-ray diffractometer (Bruker Inc., Germany). The thermal properties of GO/Alg and M-GO/Alg were investigated using a thermogravimetric analyzer (TGA, Shimadzu DTG-60, Japan), which was carried out under an air environment from 20 °C to 800 °C. The vibrating sample magnetometer (VSM) was employed to measure the mass saturation magnetization of M-GO/Alg (Quantum Design, Inc., USA). The pH of zero point charge (pH_{pzc}) was determined to evaluate the M-GO/Alg surface charge at different pH.

4. Dye Adsorption Experiments

A series of conical flasks containing 2.5 g/L M-GO/Alg and MB (100, 300, and 500 mg/L) or CV (50, 100 and 200 mg/L) were placed into a shaker at 160 rpm at room temperature. All suspensions were taken from the shaker after 360 min for MB and 600 min for CV to reach the equilibrium of adsorption. The effect of the initial pH of the solution on the dye removal was analyzed over a pH value, and the pH was adjusted with 0.1 mol/L NaOH or HCl solutions. In this research, the natural pH solution of MB and CV without adjustment by 0.1 mol/L NaOH or HCl was about 6.01 and 6.48, respectively. For single component systems, the MB and CV concentration during adsorption studies was detected by a UV-Vis spectrophotometer (Puxi TU-1810) at 665 nm and 585 nm, respectively. For the binary dye system, the dye concentration were measured as follows [43]:

$$C_A = \frac{k_{B2}A_1 - k_{B1}A_2}{k_{A1}k_{B2} - k_{A2}k_{B1}} \quad (1)$$

$$C_B = \frac{k_{A1}A_2 - k_{A2}A_1}{k_{A1}k_{B2} - k_{A2}k_{B1}} \quad (2)$$

where k_{A1}, k_{B1}, k_{A2} and k_{B2} refer to the calibration constants for dye A and B (Here, A refers to MB, and B refers to NR) at $\lambda_{1,max}$ and $\lambda_{2,max}$, respectively. A_1 and A_2 represent the absorbance at $\lambda_{1,max}$ and $\lambda_{2,max}$, respectively. The calibration curves for both dyes are shown in Fig. S1. For the adsorption kinetics, the flakes were taken from the shaker at pre-settled time intervals. Adsorption quantity of dye versus reaction time was obtained at three dye concentrations (100, 300, and 500 mg/L for MB or 50, 100 and 200 mg/L for CV). The adsorbent dose for adsorption isotherm assays was 2.5 g/L, and MB concentration was in a range of 100 to 900 mg/L, and CV concentration ranged from 20 to 200 mg/L at 298, 308, and 318 K, respectively. For binary systems, M-GO/Alg at loading of 2.5 g/L was mixed with MB and CV at various initial concentrations.

The adsorption quantity of dye (q_e, mg/g) was determined with the following equations [44]:

$$q_e = \frac{V(C_0 - C_e)}{m} \quad (3)$$

where C_0 (mg/L) and C_e (mg/L) are the initial dye concentration and equilibrium dye concentration, respectively; m (g) is the mass of adsorbent; V (L) is the solution volume. The analysis was performed in triplicate for each sample.

5. Desorption and Regeneration Experiment

Adsorbent regeneration was investigated by subjecting them to several adsorption-desorption cycles. After completing an adsorption experiment, the M-GO/Alg hybrid beads (loaded with MB or CV) were separated from the suspensions, and were added into a 0.1 mol/L HNO_3 solution (desorbing agent) by shaking 360 min for MB and 600 min for CV to recover the adsorption sites. After each adsorption-desorption cycle, desorbed composites were washed with pure water and reconditioned for MB and CV adsorption for the subsequent cycle.

RESULTS AND DISCUSSION

1. M-GO/Alg Characterization

1-1. Morphology Analysis

The spherical, millimeter-sized magnetic beads had a dark appearance as shown in Fig. S2. Fig. S3 displays the SEM of the GO, GO/Alg, and M-GO/Alg beads. The image (Fig. S3(a)) shows GO had a rolled-up edge connected with a thin wrinkled sheet, suggesting the GO has a crumpled and rippled structure and restacking has occurred [45]. The same GO stacked structure was obtained by Platero et al. [46], who reported that the non-uniformly oriented walls of GO allowed it to easily combine with alginate to produce

the composites. These results suggested that GO was successfully synthesized by our proposed method. From Fig. S3(b), GO/Alg has a rough surface on which many large pores are formed, whose irregular structure can promote the adsorption of dyes. The presence of Fe_3O_4 on the surface of M-GO/Alg is clearly observed (Fig. S3(c)), confirming the successful preparation of magnetic-GO/Alg composite beads.

1-2. XRD Analysis

XRD patterns of GO, GO/Alg and M-GO/Alg are given in Fig. S4. After encapsulation with alginate and Fe_3O_4 nanoparticles to produce the composite beads, the characteristic peaks of GO disappeared. Compared with the GO/Alg diffraction peak, all the diffraction peaks of Fe_3O_4 (18.3° (111), 30.0° (220), 35.4° (311), 43.0° (400), 53.4° (422), 56.9° (511), and 62.5° (440)) [25] were observed in the M-GO/Alg pattern, indicating the successful preparation of magnetic GO/Alg beads. Similar XRD data of GO composites have been reported by other authors [25].

1-3. Thermogravimetric (TG) Analysis Results

Thermogravimetric analysis of the GO/Alg and M-GO/Alg beads is shown in Fig. S5. Three stages could be divided according to the weight loss of both types of composite beads. In the first stage below 200 °C, the samples reveal a weight loss of 10.0 wt%; this may be explained by the fact that H_2O was evaporated and carbonaceous gases, for example, CO and CO_2, were released in this stage. These gases were formed during disproportionation reactions, which indicated there were some structural defects in GO due to the oxidation caused by strong acid [46]. In the second stage, a steeper mass loss occurred from 200-320 °C, presumably because the alginate backbone was broken and the hydroxyl groups of alginate were lost [46]. In the third stage, above 320 °C, the gradual mass loss could have been attributed to more stable functional groups [46]. Moreover, due to the introduction of Fe_3O_4 into the GO/Alg composite, the weight loss of GO/Alg beads (about 80 wt%) was much greater than that of the M-GO/Alg beads (about 40 wt%). This indicates that the addition of Fe_3O_4 increased the thermostability of the beads even at higher temperatures [2].

1-4. VSM Analysis

Fe_3O_4 endowed the GO/Alg beads with magnetic properties, which were measured by VSM. The magnetization spectrum (Fig. S6) of M-GO/Alg was obtained at room temperature. The material showed zero coercivity and remanence, indicating it was superparamagnetic [2]. The mass saturation magnetization of M-GO/Alg was 28.59 emu/g. Moreover, a hand-held magnet was employed to assess the magnetic separation effect of M-GO/Alg (Fig. S6 inset). Such an external magnetic field could completely separate M-GO/Alg beads from the aqueous solution after MB adsorption. Similar results were observed for CV adsorption (it was not shown). Based on the magnetic property of M-GO/Alg, the beads displayed good magnetization, and the adsorption post-processing can become much easier and more rapid under an external magnetic field.

1-5. The pH_{pzc} of M-GO/Alg

The point of zero charge (pzc) of M-GO/Alg is illustrated in Fig. S7. The pH_{pzc} of M-GO/Alg was 5.80. When the pH value of the solution was below 5.80, the surface of M-GO/Alg was positively charged. However, when the pH value of the solution was higher than 5.80, the surface of M-GO/Alg would acquire a negative charge.

The initial pH of the solution is an important factor affecting the process of the adsorption. According to Fig. S8, MB uptake increased from 21 mg/g to 30 mg/g with increasing in pH solution from 2.6 to 4.0. And for CV, the uptake increased from 10.5 mg/g to 14 mg/g with increasing in pH solution from 2.6 to 4.0. The point of zero charge of M-GO/Alg was 5.80. The results show that important adsorption capacity was found in $pH<pH_{pzc}$, which could be explained by the fact that the alginate has a pKa value of 3.38 for mannuronic acid and 3.65 for guluronic acid. And above these two values of pH, a negative charge can be formed on the surface of the M-GO/Alg, which makes the uptake of positive charged MB and/or CV dye important. And then the adsorbed amount becomes constant in pH value above 4.0. The M-GO/Alg is considered as good adsorbent for MB and CV as they present high stability of adsorption capacity in a large domain of pH (4-10).

2. Adsorption for Single Dye Systems

2-1. Effect of Contact Time and Initial Dye Concentration

The effects of contact time and initial dye concentration on the MB and CV adsorption by M-GO/Alg are illustrated in Fig. 1. For a given concentration, the rate of adsorption of both MB and CV increased with the contact time, and then slowed after certain minutes when the system arrived at equilibrium due to exhaustion of the adsorption sites [47]. Suggesting that two-stage kinetic behavior was evident: one stage is for the rapid adsorption, which contributes significantly to equilibrium uptake; and the other stage is for the slower adsorption, which contributes to the relatively small

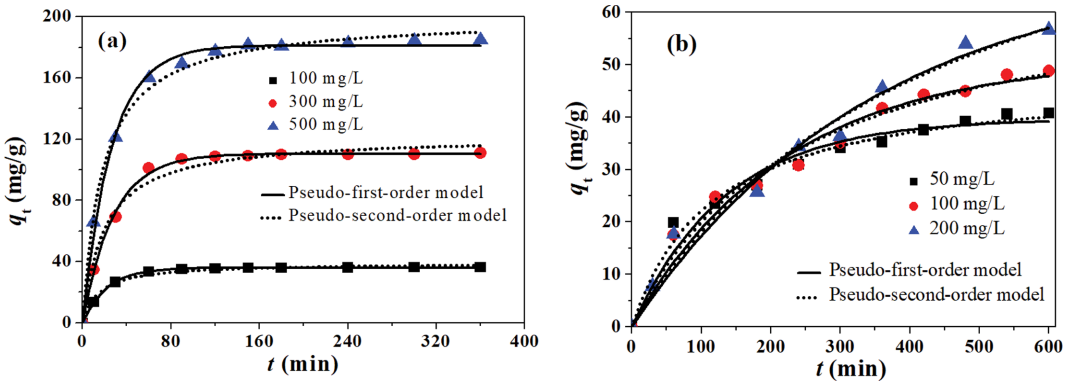

Fig. 1. The Pseudo-first-order and Pseudo-second-order kinetic models for MB (a) and CV (b) adsorption by M-GO/Alg.

MB or CV adsorption.

One can also observe that higher initial concentrations can improve higher adsorption of MB and CV on M-GO/Alg (Fig. 1(a) and 1(b)). Suggesting that the increase of concentration may decrease the boundary layer thickness surrounding the sorbent, resulting in the decreasing of the mass transfer resistance of the dyes in the boundary layer [47]. That is, higher initial concentration of dye can provide greater driving force of the adsorption, and this can produce a higher concentration gradient to overcome the MB and CV resistance when mass transfer occurs in the solutions [48].

2-2. Adsorption Kinetic Study

The pseudo-first-order and pseudo-second-order models were employed to study the MB and CV adsorption process onto M-GO/Alg. The equation of pseudo-first-order model is as follows [49]:

$$q_t = q_e(1-e^{-k_1 t}) \quad (4)$$

where q_e (mg/g) is the equilibrium adsorption quantity of dyes, and q_t (mg/g) is the adsorption quantity of dyes with time t (min), respectively, and k_1 (1/min) refers to first-order rate constant.

The pseudo-second-order kinetics model is expressed as following equation [50]:

$$q_t = \frac{k_2 q_e^2 t}{1+k_2 q_e t} \quad (5)$$

where k_2 (g/mg·min) refers to second-order rate constant.

The parameters fitted by the two models above are depicted in Fig. 1(a) and 1(b) and in Table 1. As shown in Table 1, q_t increased with the initial concentration for both MB and CV, and the correlation coefficients (R^2>0.98 for MB) were slightly different for pseudo-first-order and pseudo-second-order models, suggesting that both models can describe the kinetic process of MB adsorption on M-GO/Alg. While for CV adsorption, the pseudo-second-order model can better fit the kinetic process according to the correlation coefficients. This suggests that a chemical process, which could share the electrons or exchange electron by covalent forces between the dye and the adsorbents, may control adsorption processes [51]; the same conclusion has been reported by other authors [51]. The pseudo-second-order model suggested MB and CV adsorption may involve other chemical interactions. For example, (i) the interaction formed by free electrons of MB and CV with the delocalized π electrons of the adsorbent surface [52], or the hydrogen bonding produced by the N^+ in MB and CV interacting with the groups of -OH on the surface of adsorbent [28,52]; (ii) π-π interactions in MB and CV molecules and GO of M-GO/Alg [28,53].

One or several processes may control the overall adsorption, which cannot be described by the two models above. Thus, the intra-particle diffusion model [49] was employed to plot the data obtained from experiments, whose equation is given as follows:

$$q_t = k_t t^{1/2} + C \quad (6)$$

where k_t (g/mg·min$^{1/2}$) refers to rate constant of intra-particle diffusion, and C is a constant. The two parameters above could be obtained from a q_t versus $t^{1/2}$ plot, where k_t is the slope and C is the intercept (Table 1). Two linear regimes are shown in Fig. 2(a) for MB, indicating that two steps may occur in the process of MB adsorption: the first step is the dye diffusion from solution to the external surface of the adsorbents; and gradual adsorption stage occurs in the second step for dye removal by adsorbents until equilibrium. This step is rate-limiting of the intra-particle diffusion. The first linear segment (Fig. 2(a)) may be due to the first step, and the second segment (Fig. 2(a)) may represent the second step. The gradual adsorption stage of the second segment can be explained by noting that MB was slowly transported in the particles through intra-particle diffusion before being retained in the micropores [54]. The value of k_{t1} increased from 4.29 to 16.66 mg/g·min$^{1/2}$ with the initial concentration for MB adsorption onto M-GO/Alg. However, unlike the case of MB adsorption, the CV adsorption exhibits a one-stage diffusion process (Fig. 2(b)). And the k_{t1} values de-

Table 1. Kinetic constants for MB and CV adsorption on M-GO/Alg in single systems

For MB				For CV			
Parameters	$C_{0,MB}$/(mg/L)			Parameters	$C_{0,CV}$/(mg/L)		
	100	300	500		50	100	200
Pseudo-first-order model							
q_t (mg/g)	35.97±0.001	110.48±0.001	181.21±0.15	q_t (mg/g)	39.66±1.42	51.18±2.85	69.44±8.51
k_1 (min^{-1})	0.046±0.001	0.036±0.001	0.038±0.001	k_1 (min^{-1})×10^3	7.39±0.95	4.54±0.64	2.87±0.63
R^2	0.999	0.998	0.996	R^2	0.966	0.972	0.977
Pseudo-second-order model							
q_t (mg/g)	39.13±0.51	122.11±1.12	199.50±1.46	q_t (mg/g)	47.85±1.85	67.51±4.71	100.03±15.53
k_2×10^3 (g/mg·min)	1.73±0.22	0.42±0.08	0.28±0.09	k_2×10^3 (g/mg·min)	0.18±0.03	0.60±0.02	0.02±0.001
R^2	0.990	0.982	0.996	R^2	0.985	0.980	0.979
Intraparticle diffusion model							
k_{t1} (mg/g·min$^{1/2}$)	4.29	14.49	16.66	k_{t1} (mg/g·min$^{1/2}$)	10.41	2.08	2.54
C	1.09	−10.83	21.26	C	1.31	1.97	−4.71
R	0.986	0.999	0.974	R	0.981	0.991	0.982

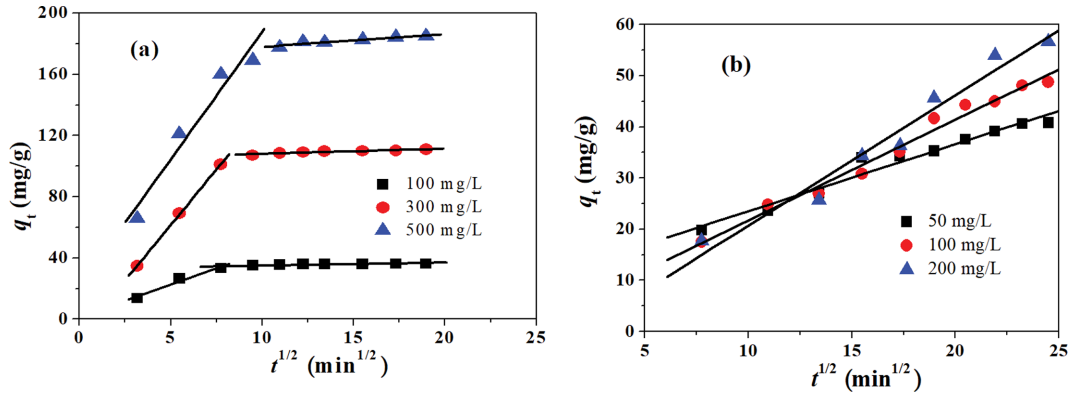

Fig. 2. Intra-particle diffusion plots for MB (a) and CV (b) adsorption onto M-GO/Alg (Note: The two straight black lines on the experimental points in the Fig. 2(a) were plotted by the intra-particle diffusion model).

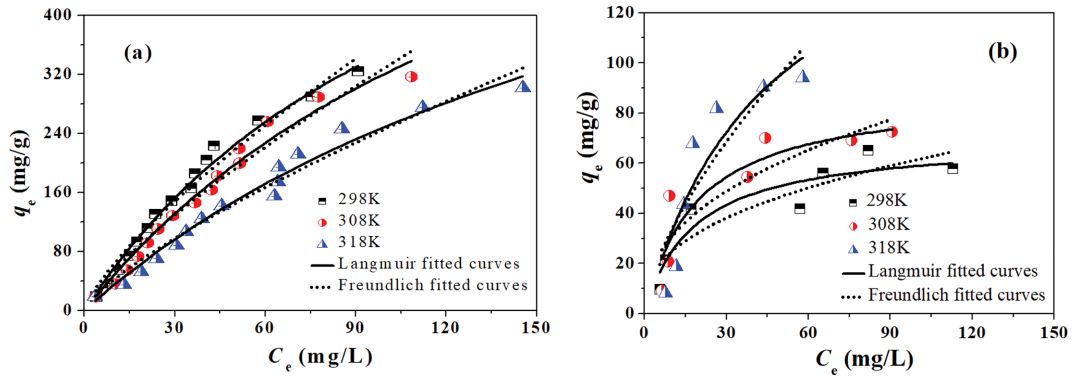

Fig. 3. The non-linear fitted curves with Langmuir and Freundlich models for adsorption of MB (a) and CV (b) on M-GO/Alg.

creased with the initial concentration for CV. The different behavior of both dyes may be attributed to the difference in molecular size [47]. As shown in Fig. 2(a) and Fig. 2(b), the line does not pass through the origin, and this may be explained by the fact that a boundary layer resistance may occur between the dye and the composite beads.

2-3. Effect of Equilibrium Concentration of MB and CV on Temperature-dependent Adsorption

The equilibrium adsorption at different initial concentration of MB and CV is shown in Fig. 3. One can observe that the q_e values increase with the initial concentration of MB and CV dyes. This can be attributed to the fact that the initial concentration can enhance the interaction between dyes and adsorbents, and it can also provide the driving forces to overcome the resistances to the mass transfer of dyes between the aqueous and solid phases [47].

The effect of temperature was also evaluated for both MB and CV. For MB, adsorption was more favorable at lower temperatures; it may be explained by the fact that higher temperature could weaken the electrostatic interaction between MB and the adsorbents. While M-GO/Alg exhibited better CV adsorption at higher temperatures, similar results were also observed by other authors [46]. The adsorption of MB was exothermic, whereas the adsorption of CV was endothermic.

Adsorption isotherms are important for the adsorption process. Both Langmuir and Freundlich models (Eq. (7) and (8)) were employed to describe adsorption isotherms, which are given as follows [49]:

$$q_e = \frac{q_{max} K_L C_e}{1 + K_L C_e} \tag{7}$$

$$q_e = K_F C_e^{1/n} \tag{8}$$

where q_e is the equilibrium sorption capacity (mg/g); C_e is the equilibrium dye concentration (mg/L); q_{max} is the maximum adsorption capacity (mg/g) obtained from Langmuir model; K_L is the Langmuir constant or binding constant (L/mg). A higher K_L suggests a higher affinity for binding sites [48]; K_F is the adsorption parameter obtained from Freundlich model, where a higher K_F indicates a higher affinity between the dye and the adsorbents [54]; and 1/n is related to the adsorption intensity [54]; favorable adsorption can occur when $0.1<1/n<1$ [54].

The fitted curves obtained from both models above at three temperatures for MB and CV are, respectively, depicted in Fig. 3. The parameters fitted from both models are listed in Table 2. From Fig. 3(a), the adsorption of MB and CV onto M-GO/Alg fits both models well. The q_{max} of MB and CV obtained from Langmuir model was 460.0 mg/g and 69.5 mg/g at 298 K, respectively. In the Freundlich isotherm model, all 1/n values lie in the interval $0.1<1/n<1$ (Table 2), suggesting that favorable adsorption can occur during the adsorption process [54]. The K_F, related to the adsorp-

Table 2. Isotherm parameters of adsorption of MB and CV onto M-GO/Alg in single dye solution

For MB				For CV			
Parameters	T/K			Parameters	T/K		
	298	308	318		298	308	318
Langmuir constants							
q_m (mg/g)	459.85±5.24	419.43±9.82	363.84±8.29	q_m (mg/g)	69.46±8.73	88.86±15.05	182.08±7.49
K_L (L/mg)×10^3	4.50±0.32	2.46±0. 23	2.91±0.12	K_L (L/mg)	0.055±0.025	0.053±0.027	0.022±0.016
R^2	0.987	0.979	0.979	R^2	0.877	0.833	0.831
Freundlich constants							
K_F	8.69±3.02	6.40±1.26	5.81±1.29	K_F	9.92±4.49	11.77±5.70	12.39±4.84
1/n	0.76±0.13	0.78±0.12	0.77±0.15	1/n	0.40±0.10	0.42±0.12	0.66±0.18
R^2	0.973	0.964	0.967	R^2	0.833	0.783	0.782

Table 3. Thermodynamic parameters for MB and CV adsorption

Dyes	ΔG^o (kJ/mol)			ΔH^o (kJ/mol)	ΔS^o (J/mol·K)
	298 K	308 K	318 K		
MB	−6.40	−6.01	−5.41	−21.12	−49.30
CV	−3.08	−3.25	−3.69	−0.66	8.7

tion capacity, decreased with temperature for MB, whereas increased with temperature for CV, suggesting adsorption was exothermic for MB and endothermic for CV, which was consistent with the results of the effect of temperature.

2-4. Thermodynamics of the Adsorption

To evaluate the inherent energy changes (the free energy change ΔG^o, kJ/mol; enthalpy change ΔH^o, kJ/mol; and entropy change ΔS^o, kJ/mol·K), the adsorption thermodynamics were also investigated. The thermodynamic parameters were determined as follows [55]:

$$K_c = \frac{C_a}{C_e} \tag{9}$$

$$\Delta G^o = -RT\ln K_c \tag{10}$$

$$\Delta G^o = \Delta H^o - T\Delta S^o \tag{11}$$

where K_c is the adsorption distribution coefficient, C_a (mg/L) is the equilibrium dye amount adsorbed by the adsorbent, C_e (mg/L) represents the equilibrium dye concentration in solution. R is 8.314 J/mol·K, and T (K) is the temperature of the absorption systems.

The obtained parameters of ΔG^o, ΔH^o, and ΔS^o are listed in Table 3. According to negative ΔG^o values of MB and CV (Table 3), the spontaneous process occurred during the adsorption of both dyes onto M-GO/Alg. Negative ΔH^o and ΔS^o values for MB implied that an exothermic process and a decreasing randomness occurred at the solid-liquid interface [26]. Positive values of ΔH^o and ΔS^o values for CV suggest different adsorption mechanisms onto M-GO/Alg. Similar observations were also found by other authors, who reported that the dye adsorption process on sodium alginate immobilized graphene oxide was endothermic [46].

2-5. Desorption and Regeneration of M-GO/Alg

The regeneration of spent adsorbents and the recovery of adsorbate are important to practical applications of wastewater treatment. Therefore, the dye adsorption capacity of M-GO/Alg was investigated by five repeated adsorption-desorption cycles using M-GO/Alg for MB and CV removal (Fig. 4). The removal efficiency of MB and CV onto the two adsorbents slightly decreased after five cycles but still remained high at 90%. The results indicate that the M-GO/Alg can be used as efficient adsorbent due to excellent regeneration performance.

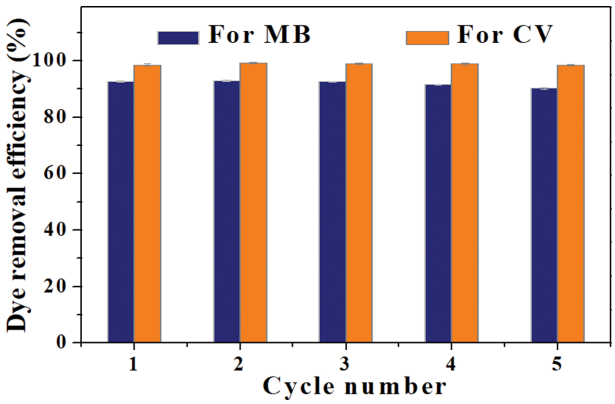

Fig. 4. Reusability of M-GO/Alg composite for MB and CV removal.

3. Adsorption for Binary MB and CV Dye Systems

3-1. Effect of MB or CV Adsorption with the Presence of CV or MB in the System

In the binary system, the initial concentration of MB (primary dye) was fixed to 300 mg/L, whereas the CV (interferential dye) concentration ranged from 20 to 200 mg/L; or the initial concentration of CV (primary dye) was fixed to 200 mg/L and the MB (interferential dye) concentration ranged from 50 to 500 mg/L.

The 3D isotherm surfaces for adsorption quantity versus the equilibrium concentration of MB and CV are depicted in Fig. 5. The adsorption of the primary dye was decreased with the increasing initial concentrations of the interferential dye. From Fig. 5, the interference of CV with the MB adsorption is more obvious. The q_e values of MB decreased from 111.6 to 40.4 mg/g (reduction of 63.8%) in the presence of CV, while the q_e values of CV increased from 29.3 to 40.7 mg/g (increment of 38.9%) in the presence of MB. However, it was still less than that of CV in the single systems, which coincided with the conclusion derived from Fig. 3. Thus, compared to MB, CV had a better affinity for M-GO/Alg.

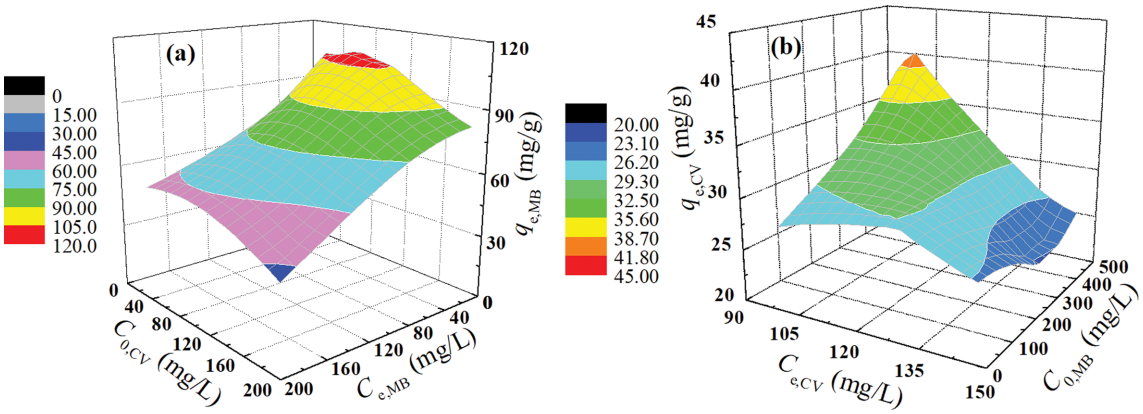

Fig. 5. 3D isotherm surfaces of the MB/CV coadsorption system. (a) Adsorption capacity of MB is plotted as a function of the equilibrium concentrations of MB and (b) Adsorption capacity of CV is plotted as a function of the equilibrium concentrations of CV.

3-2. The Competitive Adsorption of MB and CV with a Fixed Total Concentration

In the binary system, the total concentration of MB and NR was fixed at 300 mg/L and each dye concentration was changed at 298 K. The experimental results are depicted in Fig. 6. As shown, one can observe that the q_e values of MB or CV in the binary system are lower than that in single dye system, suggesting that MB or CV can inhibit the adsorption yield of each other. However, the total adsorption uptake for both dyes in binary system exceeded the capacity of MB or NR in single systems (Table 2), suggesting that competitive adsorption exists between MB and CV in the binary system.

4. Possible Adsorption Mechanism Analysis

In this study, the plausible adsorption mechanisms of MB and CV onto M-GO/Alg were mainly associated with electrostatic interaction, hydrogen bonding and π-π interactions. For example, the interaction formed by free electrons of MB and CV with the delocalized π electrons of the adsorbent surface [52], or the hydrogen bonding produced by the N^+ in MB and CV interacting with the groups of -OH on the surface of adsorbent [28,52]; π-π interactions in MB and CV molecules and GO of M-GO/Alg [28,53]. In the co-adsorption system, the benzene rings in the MB and CV molecules could form the π-π stacking interaction, and the specific sites on the surface of the adsorbents could be partially overlapped with MB and CV due to the competitive adsorption of both dyes.

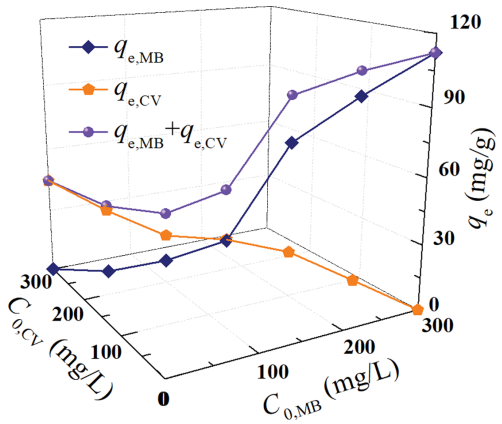

Fig. 6. Effect of the fixed total initial concentration of MB and CV on the adsorption capacity of each adsorbate.

CONCLUSIONS

Thhe preparation of magnetic alginate composite beads containing iron oxide nanoparticles and graphene oxide was reported. The composites were used as adsorbents to study their adsorption kinetics, isotherms of MB and CV from aqueous solutions in single and binary systems. For the single system, the adsorption processes were well described by the three kinetic models. The experimental data for MB and CV followed well by both Langmuir and Freundlich models, and M-GO/Alg exhibited high adsorption capacity with q_{max} values of 459.85 and 69.46 mg/g at 298 K for MB and CV, respectively. The process mechanism for both dyes adsorption to the adsorbent was found to be complex. Furthermore, MB or CV desorption was achieved using HNO_3 as a desorbing agent. The adsorbents were used in five successive adsorption-desorption cycles with high regeneration and stability, which suggested that the adsorbent was stable with excellent reusability. In a binary system, MB and CV show competitive adsorption and CV exhibits higher affinity to the adsorbent. The obtained results have provided insights into efficient and renewable adsorbent design for dye-contaminated water treatment.

ACKNOWLEDGEMENTS

The authors would like to acknowledge the financial support provided by research funds from the financial support of National Natural Science Foundation of China (No. 41807120), the Cultivation Plan for Young Core Teachers in Universities of Henan Province (No. 2021GGJS063), the Fundamental Research Funds for the Henan Provincial Colleges and Universities in Henan University of Technology (No. 2018QNJH01), Doctor Foundation of Henan University of Technology (No. 2018BS003), Science and Technology Foundation of Henan Province (No. 212102310026; No. 202102310208) and the Young Backbone Teachers Training Program Foundation of Henan University of Technology.

SUPPORTING INFORMATION

Additional information as noted in the text. This information is available via the Internet at http://www.springer.com/chemistry/journal/11814.

REFERENCES

1. A. Nasar and F. Mashkoor, *Environ. Sci. Pollut. Res.*, **26**, 5333 (2019).
2. B. Chen, S. J. Chen, H. N. Zhao, Y. Liu, F. X. Long and X. J. Pan, *Chemosphere*, **216**, 605 (2019).
3. W. Y. Qu, T. Yuan, G. J. Yin, S. A. Xu, Q. Zhang and H. J. Su, *Fuel*, **249**, 45 (2019).
4. A. Sandoval, C. H. Ventura and T. E. Klimova, *Fuel*, **198**, 22 (2017).
5. C. Y. Tsai, C. W. Liu, H. C. Hsi, K. S. Lin, Y. W. Lin, L. C. Lai and T. N. Weng, *Environ. Sci. Pollut. Res.*, **26**, 22082 (2019).
6. R. Paradelo, X. Vecino, A. B. Moldes and M. T. Barral, *Environ. Sci. Pollut. Res.*, **26**, 21085 (2019).
7. B. Chen, H. N. Zhao, S. J. Chen, F. X. Long, B. Huang, B. Q. Yang and X. J. Pan, *Chem. Eng. J.*, **356**, 69 (2019).
8. A. Roy, B. Adhikari S. B. Majumder, *Ind. Eng. Chem. Res.*, **52**, 6502 (2013).
9. C. A. Matias, P. B. Vilela, V. A. Becegato and A. T. Paulino, *Int. J. Environ. Res.*, **13**, 991 (2019).
10. R. F. Wang, L. G. Deng, K. Li, X. J. Fan, W. Li and H. Q. Lu, *Ceram. Int.*, **46**, 27484 (2020).
11. Y. H. Wu, K. Xue, Q. L. Ma, T. Ma, Y. L. Ma, Y. G. Sun and W. X. Ji, *Micropor. Mesopor. Mater.*, **312**, 110742 (2021).
12. S. Pashaei-Fakhri, S. J. Peighambardoust, R. Foroutan, N. Arsalani and B. Ramavandi, *Chemosphere*, **270**, 129419 (2021).
13. H. Hou, R. Zhou, P. Wu and L. Wu, *Chem. Eng. J.*, **211-212**, 336 (2012).
14. M. Bergaoui, A. Nakhli, Y. Benguerba, M. Khalfaoui, A. Erto, F. E. Soetaredjo, S. Iamadji and B. Ernst, *J. Mol. Liq.*, **272**, 697 (2018).
15. P. Liu, C. Milletto, S. Monti, C. Zhu and A. P. Mathew, *RSC Adv.*, **9**, 28657 (2019).
16. A. Aher, S. Thompson, T. Nickerson, L. Ormsbee and D. Bhattacharyya, *RSC Adv.*, **9**, 38547 (2019).
17. S. Ramanayaka, M. Vithanage, A. Sarmah, T. An, K.-H. Kim and Y. S. Ok, *RSC Adv.*, **9**, 34359 (2019).
18. R. Azmat, A. Khursheed, A. Saleem and N. Qamer, *RSC Adv.*, **9**, 37562 (2019).
19. B. Zheng, Y. Ye, B. Hu, C. Luo and Y. Zhu, *RSC Adv.*, **9**, 36144 (2019).
20. J. Cheng, P. R. Chang, P. W. Zheng and X. F. Ma, *Ind. Eng. Chem. Res.*, **53**, 1415 (2014).
21. J. Q. Bu, L. Yuan, N. Zhang, Y. Meng and X. Peng, *J. Chem. Eng. Data*, **66**, 199 (2021).
22. J. F. Du, X. Yang, H. H. Xiong, Z. Dong, Z. W. Wang, Z. Y. Chen and L. Zhao, *J. Chem. Eng. Data*, **66**, 1264 (2021).
23. Z. Esmaeili, S. Izadyar, Y. Hamzeh and A. Abdulkhani, *J. Chem. Eng. Data*, **66**, 1068 (2021).
24. L. Liu, B. Zhang, Y. R. Zhang, Y. J. He, L. H. Huang, S. Z. Tan and X. Cai, *J. Chem. Eng. Data*, **60**, 1270 (2015).
25. M. M. Gao, Z. M. Wang, C. X. Yang, J. L. Ning, Z. D. Zhou and G. Y. Li, *Colloids Surf. A*, **566**, 48 (2019).
26. A. Mohammadi, A. H. Doctorsafaei and K. M. Zia, *Int. J. Biol. Macromol.*, **120**, 1353 (2018).
27. S. Luo and J. L. Wang, *Environ. Sci. Pollut. Res.*, **25**, 5521 (2018).
28. Z. B. Wu, H. Zhong, X. Z. Yuan, H. Wang, L. L. Wang, X. H. Chen, G. M. Zeng and Y. Wu, *Water Res.*, **67**, 330 (2014).
29. S. Raza, X. Y. Yong, M. Raza and J. P. Deng, *Chem. Eng. J.*, **352**, 20 (2018).
30. F. Ahmadpoor, S. A. Shojaosadati and S. Z. Mousavi, *Int. J. Biol. Macromol.*, **128**, 941 (2019).
31. C. M. Su, *J. Hazard. Mater.*, **322**, 48 (2017).
32. N. Boukhalfa, M. Boutahala, N. Djebri and A. Idris, *Int. J. Biol. Macromol.*, **123**, 539 (2019).
33. A. G. Pershina, A. E. Sazonov and V. D. Filimonov, *Russ. Chem. Rev.*, **83**, 299 (2014).
34. N. Singh, G. Jenkins, R. Asadi and S. H. Doak, *Nanotechnol. Rev.*, **1**, 5358 (2010).
35. R. Ianos, C. Pacurariu, S. Gabriela Muntean, E. Muntean, M. A. Nistor and D. Niznansky, *J. Alloys Compd.*, **741**, 1235 (2018).
36. M. Zahoor and F. A. Khan, *Arab. J. Chem.*, **11**, 729 (2018).
37. Y. Zhuang, F. Yu, J. H. Chen and J. Ma, *J. Environ. Chem. Eng.*, **4**, 147 (2016).
38. R. R. Pawar, Lalhmunsiama, P. Gupta, S. Y. Sawant, B. Shahmoradi and S. M. Lee, *Int. J. Biol. Macromol.*, **114**, 1315 (2018).
39. D. Qian, L. Bai, Y. S. Wang, F. Song, X. L. Wang and Y. Z. Wang, *Ind. Eng. Chem. Res.*, **58**, 13133 (2019).
40. B. Wang, B. Gao, A. R. Zimmerman and X. Q. Lee, *Chem. Eng. Res. Des.*, **133**, 235 (2018).
41. A. Nasrullah, A. H. Bhat, A. Naeem, M. H. Isa and M. Danish, *Int. J. Biol. Macromol.*, **107**, 1792 (2018).
42. W. S. Hummers and R. E. Offerman, *J. Am. Chem. Soc.*, **80**, 1339 (1958).
43. H. J. Bai, J. H. Chen, Z. T. Wang, L. J. Wang and E. Lamy, *J. Chem. Eng. Data*, **65**, 4443 (2020).
44. L. J. Li, F. Q. Liu, X. S. Jing, P. P. Ling and A. M. Li, *Water Res.*, **45**, 1177 (2011).
45. C. J. Fu, G. G. Zhao, H. J. Zhang and S. Li, *Int. J. Electrochem. Sci.*, **8**, 6269 (2013).
46. E. Platero, M. E. Fernandez, P. R. Bonelli and A. L. Cukierman, *J. Colloid Interface Sci.*, **491**, 1 (2017).
47. W. Zou, H. Bai, S. Gao, X. Zhao and R. Han, *Desalin. Water Treat.*, **49**, 41 (2012).
48. W. H. Zou, H. J. Bai, S. P. Gao and K. Li, *Korean J. Chem. Eng.*, **30**, 111 (2013).
49. H. M. Jang, S. Yoo, Y. K. Choi, S. Park and E. Kan, *Bioresour. Technol.*, **259**, 24 (2018).
50. S. Saruchi, V. Kumar, B. S. Kaith and R. Jindal, *Ind. Eng. Chem. Res.*, **55**, 10492 (2016).
51. Y. H. Li, Q. J. Du, T. H. Liu, J. K. Sun, Y. H. Wang, S. L. Wu, Z. H. Wang, Y. Z. Xia and L. H. Xia, *Carbonhyd. Polym.*, **95**, 501 (2013).
52. B. Wang, Y. B. Zhai, T. F. Wang, S. H. Li, C. Peng, Z. X. Wang, C. T. Li and B. B. Xu, *Bioresour. Technol.*, **274**, 525 (2019).
53. Y. Wang, W. Wang and A. Wang, *Chem. Eng. J.*, **228**, 132 (2013).
54. L. Liu, Y. Z. Wan, Y. D. Xie, R. Zhai, B. Zhang and J. D. Liu, *Chem. Eng. J.*, **187**, 210 (2012).
55. M. Barylak, K. Cendrowski and E. Mijowska, *Ind. Eng. Chem. Res.*, **57**, 4867 (2018).

Supporting Information

Renewable magnetic alginate-graphene oxide hybrid for efficient cationic dye removal

Wenju Liu, Hongjuan Bai, Weiqiang Gao, Zihan Chen, Zhuangzhuang Liu, Zilong Chen, and Junhang Chen†

School of Chemistry and Chemical Engineering, Henan University of Technology, Zhengzhou 450001, P. R. China
(*Received 9 February 2022 • Revised 4 April 2022 • Accepted 10 April 2022*)

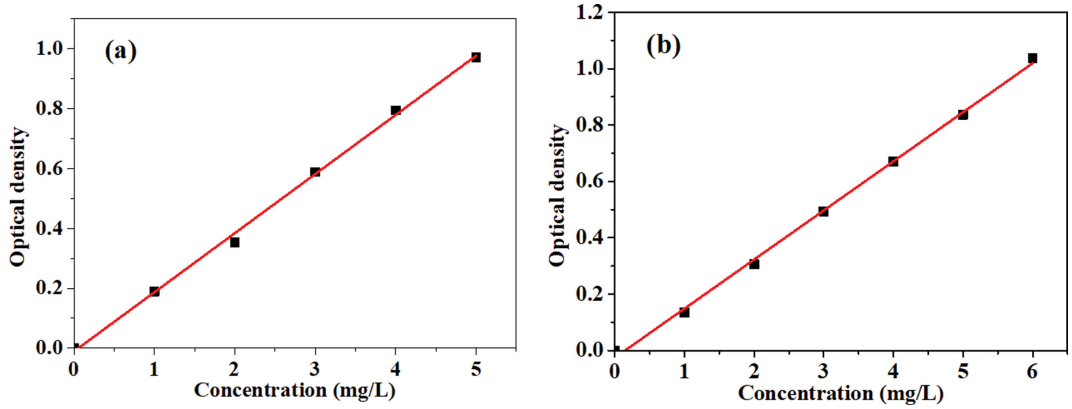

Fig. S1. The calibrate curves for MB (a) and CV (b).

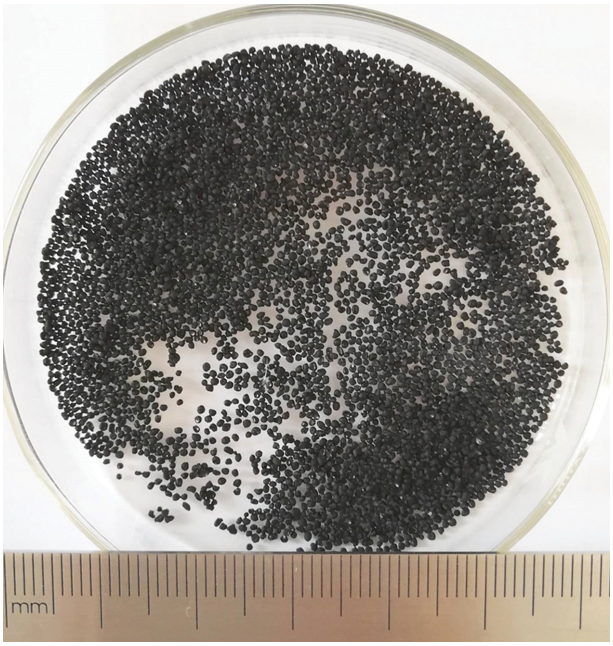

Fig. S2. Photograph of M-GO/Alg composite beads.

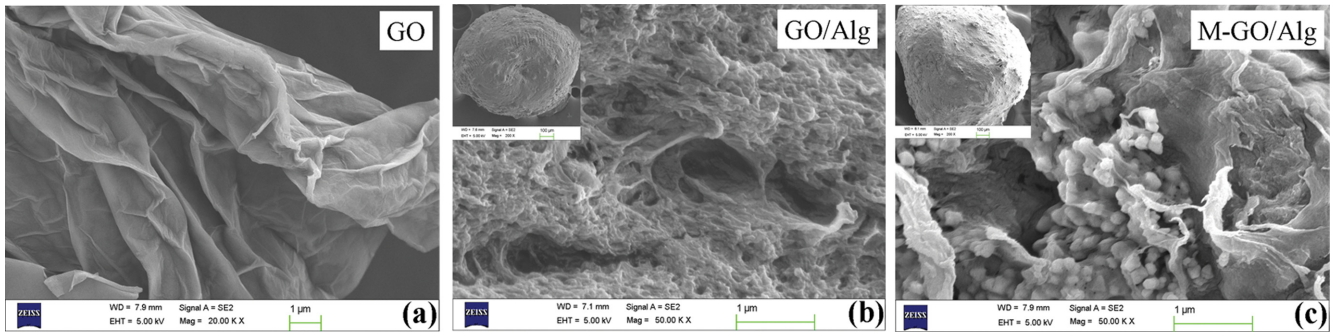

Fig. S3. Surface morphology of (a) the synthesized GO, (b) GO/Alg and (c) M-GO/Alg.

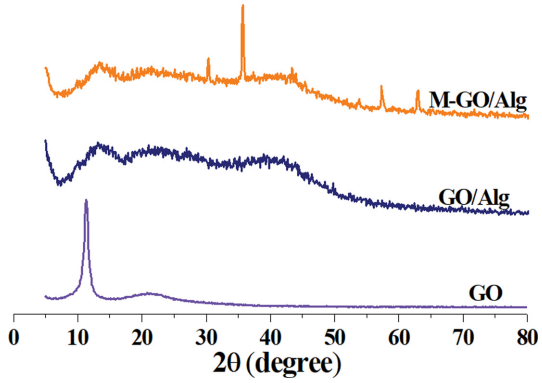

Fig. S4. XRD patterns of GO, GO/Alg and M-GO/Alg.

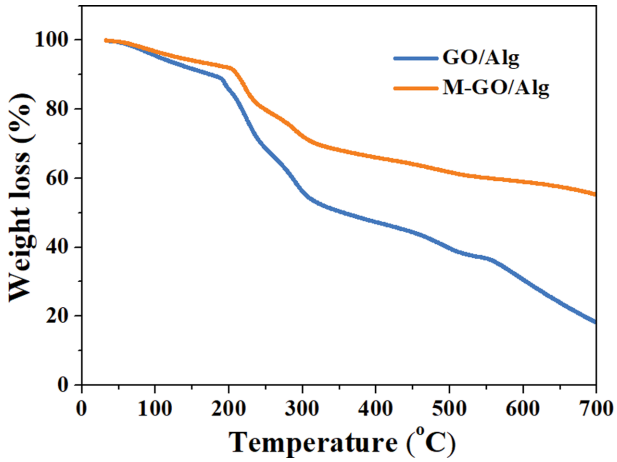

Fig. S5. TG thermograms of prepared GO/Alg and M-GO/Alg beads.

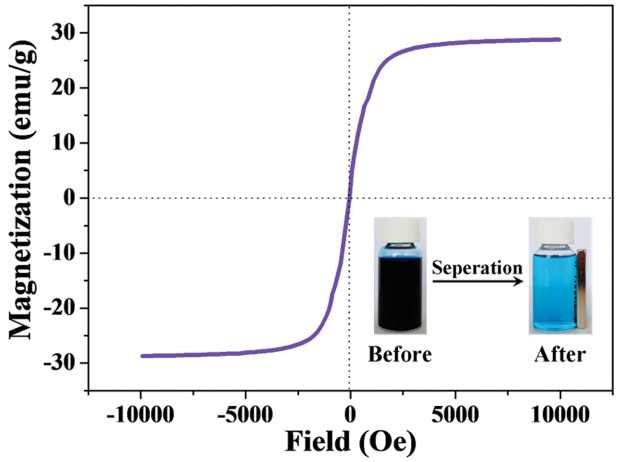

Fig. S6. Magnetization curve and demonstration of magnetic separation (inset) of M-GO/Alg.

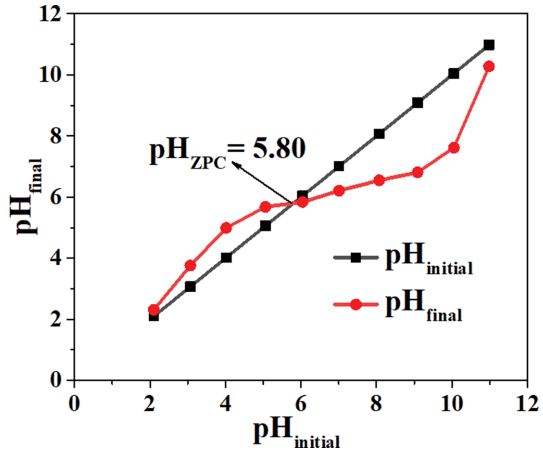

Fig. S7. Variation of zero charges with equilibrium pH of M-GO/Alg suspensions.

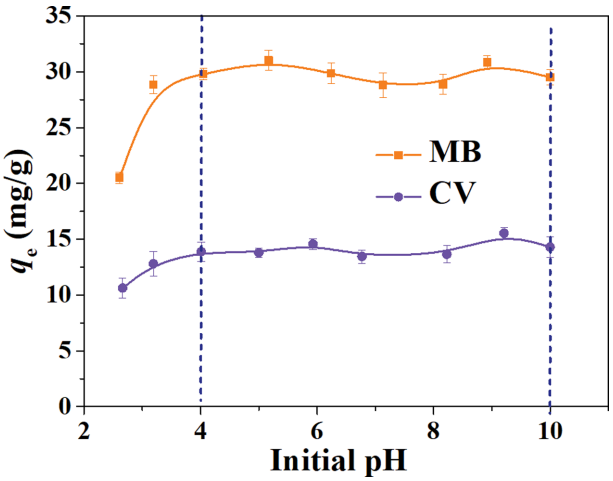

Fig. S8. Effect of pH on MB and CV adsorption onto M-GO/Alg (The initial concentration of MB and CV is 100 mg/L; the dose of adsorbent is 2.5 g/L).